Journal of Thermal Analysis and Calorimetry, Vol. 62 (2000) 277–284

TEMPERATURE-PROGRAMMED REDUCTION OF METAL-EXCHANGED ZEOLITE-A CATALYSTS

M. Afzal[1]*, G. Yasmeen*[1]*, M. Saleem*[1] *and J. Afzal*[2]

[1]Department of Chemistry, Quaid-i-Azam University, Islamabad
[2]National Institute for Biotechnology and Genetic Engineering, P.O. Box 577, Faisalabaad
Pakistan

(Received January 17, 1999; in revised form October 30, 1999)

Abstract

The reduction of metal (Co, Ni, and Cu)-exchanged zeolite-A was studied by a temperature-programmed reduction (TPR) technique. The TPR profiles indicate that the metals are in a dispersed form. The hydrogen consumption in the reduction process demonstrates that the metals are present in monovalent and divalent forms. High-temperature reduction peaks are also observed in the cases of CoA and NiA. Nitrogen adsorption reveals that, on heating at high temperature, the pore capacity of zeolite-A increases when exchanged with transition metals because more space is occupied by water molecules. This is confirmed by thermal analysis. After dehydration, the cations are in changed positions; they are often located in hidden sites (hexagonal prism and sodalite cages). The activation energy for the reduction process is calculated.

Keywords: TPR technique, transition metal-exchanged zeolites, zeolite-A catalysts

Introduction

Transition metal ion-exchanged zeolites can be used as catalysts for a wide range of chemical reactions, including dehydrogenation, oxidation, isomerization and the cracking of various organic feed stocks. The metal must usually be present in the zero-valent oxidation state, which can be accomplished by hydrogen reduction at elevated temperatures [1, 2]. Transition metal-exchanged zeolites, in either unreduced or reduced form, are powerful catalysts for a wide range of organic reactions, including selective oxidation, hydrogenation and isomerization [3]. Transition metals highly dispersed in zeolites are commercially available as hydrocracking catalysts [4]. The reductions of supported metals are currently receiving considerable attention due to their widespread industrial importance as catalysts [5, 6]. TPR techniques have been extensively applied to study the reducibility of supported metals under different conditions [7]. In TPR, the supported or unsupported metal oxide is reduced by flowing hydrogen, usually mixed with some inert gas such as argon, nitrogen or helium. The technique makes use of the high thermal conductivity of hydrogen. The choice of

1418–2874/2000/ $ 5.00

Akadémiai Kiadó, Budapest
Kluwer Academic Publishers, Dordrecht

the other component (inert gas) is usually made by considering its reactivity and thermal conductivity. The thermal conductivity of this gas should be quite different from that of hydrogen. The thermal conductivity of nitrogen is not very different from those of other inert gases. Thus, nitrogen is the most suitable choice and a reducing gas mixture is usually allowed to pass through the reactor containing the solid catalyst to reduce the metal oxide into metallic atoms. TPR studies have earlier been carried out on silica-supported platinum and metal-supported active carbon in our laboratory [8, 9].

Experimental

Zeolite-4A was supplied by Merck. It was ground in an agate mortar and passed through U.S. standard sieve series no. 140 having a mesh size of 105 micron. The metal(II) chlorides used were supplied by Merck with a purity better than 99%.

Metal-exchanged sample were prepared by magnetically stirring a predetermined amount of metal chloride and zeolite-4A in 100 ml distilled water at different temperatures and time intervals. The amount of metal exchanged was determined by an EDTA microtitration method.

Nitrogen adsorption isotherms were measured at 77 K by using a Quantasorb sorption system, and surface area was calculated by the BET method. Before adsorption measurements, samples were heated at 100 or 300°C. Pore size distribution was determined by using an Autopore II 9220 mercury porosimeter. The exact number of water molecules was detected by using a Shimadzu thermal analyzer.

For TPR measurements, an accurately weighed sample was taken in a gradientless U-shaped quartz reactor. The reactor was connected to the rest of the system and placed inside the furnace at a temperature low enough to prevent reaction (usually at room temperature), and a reducing gas mixture (6% hydrogen in nitrogen) was allowed to flow through the system at a flow rate of 40 ml min^{-1}. At this stage, the whole system was checked for leaks. A temperature-programmed furnace was used at a heating rate of 8°C min^{-1} and the detector current was adjusted to 16 mA.

Experimental details were entered into a computer program especially designed for TPR. A suitable amplifier gain was chosen and the system was left to stabilize for about half an hour in order to obtain a straight baseline. Once the straight baseline had been obtained, the reduction of the solid was started by switching on the temperature-programmed furnace. The hydrogen consumption was monitored with a thermoconductivity detector connected to a personal computer for data storage and processing.

Before all TPR tests, the samples were heated at 250°C for 4 h, then cooled to room temperature and purged in a nitrogen flow.

After reduction, the whole system was calibrated by injecting a known volume of hydrogen into the detector (hydrogen sampling loop of 0.125 ml).

Results and discussion

From the nitrogen adsorption data, it is evident that, as the temperature of outgassing is increased, the capacity of the zeolite cavity also increases after exchange with metals, because most of the space is occupied by water molecules. From the thermal analysis data, it can be seen that, after exchange with transition metal, the number of water molecules increases, which may be due to the hydrated ionic radii of the metals. The nitrogen adsorption and thermal data are given in Tables 1 and 2, respectively. After dehydration, cations move towards the walls of the aluminosilicates [10]. It is known that, after dehydration, zeolite cations are often located in hidden sites (hexagonal prism and sodalite cages) [11]. Zeolites containing reduced metal, whether atomically dispersed or as small clusters within the pore structure, are of great value in the petrochemical industry as hydrocracking and reforming catalysts [12]. The activity of these catalysts is critically dependent on both the degree of dispersion and the location of the metal, which are in turn dependent on the method of reduction and pretreatment. Thus, an understanding of the kinetics and mechanism of reduction is particularly valuable as concerns the preparation of these catalysts.

Table 1 Nitrogen adsorption data for NaA zeolite and metal-exchanged zeolite

Sample	Specific surface area/$m^2\ g^{-1}$			
	After outgassing at 100°C		After outgassing at 300°C	
	Single point method	BET method	Single point method	BET method
NaA	38.61	115.05	43.56	129.21
CoA	30.78	93.68	98.64	185.82
NiA	29.67	76.63	91.47	180.80
CuA	28.45	30.85	45.43	151.47

Table 2 Kinetic parameters for dehydration of metal-exchanged zeolite-A

Sample	DTA T_{max}/°C	Mass loss/%	No. of water molecules	Activation energy/ kJ mol^{-1}
NaA	125	22.2	27	15.36
CoA	112	24.8	30	13.51
NiA	110	25.4	31	12.80
CuA	112	23.4	29	12.43

The reduction of a metal ion in a zeolite is generally achieved by using hydrogen; the overall reaction stoichiometry may be written [13] as:

$$M^{n+} + n/2H_2 \rightarrow M^o + nH^+ \quad (1)$$

The protons react with the zeolite lattice to produce hydroxy groups, whose presence has been established by IR spectroscopy [14]:

$$nZO^- + nH^+ \rightarrow nZOH \quad (2)$$

The reduction of transition metal ions in zeolites was reviewed by Utterhoeven [13], who observed a correlation between the reducibility and the standard electrode potential. Briend-Faure *et al.* [15] studied the reduction of Ni^{2+} in both X and Y zeolites. In NiY, they observed three distinct kinetic regimes dependent on both the initial level of exchange and the degree of reduction, and they correlated these reduction regimes to the initial distribution of Ni^{2+}. In all the foregoing work on the Ni^{2+} zeolite systems, Ni^o was found to be the only reduction product. Using EPR and electron spectroscopy, however, Garbowski *et al.* [16, 17] observed Ni^+. TPR at relatively high hydrogen pressure [13] did not reveal a two-step mechanism; hence, it must be assumed that the concentration of Ni^+ is low and that further reduction to Ni^o is rapid. According to Barthomeuf [18], the reduction by hydrogen of transition metal cations in zeolites was presumed to form a hydrogen zeolite. Such Bronsted acidity has been observed in the IR spectroscopy of hydrogen-reduced Cu^{2+}Y zeolite [19].

$$\begin{aligned} 2Cu^{2+} + H_2 &\rightarrow 2Cu^+ + 2H^+ \\ 2Cu^+ + H_2 &\rightarrow 2Cu^o + 2H^+ \end{aligned} \quad (3)$$

Literature on the reduction of transition metals in zeolites X and Y is readily available [20–27], but literature on NaA zeolite is scanty [28].

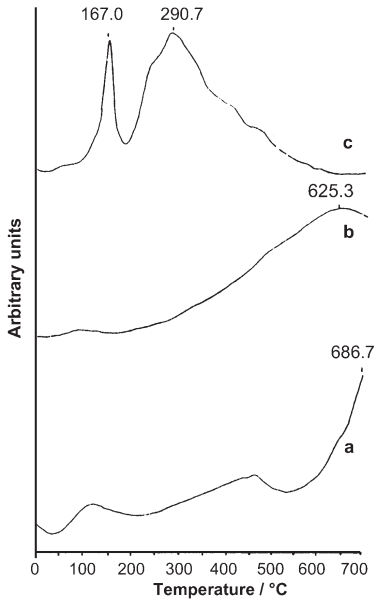

Fig. 1 TPR profiles of a – CoA; b – NiA and c – CuA

TPR profiles for CoA, NiA and CuA are given in Fig. 1. There is only a single reduction peak in the cases of CoA and NiA. A few literature data are available on the reduction of Co^{2+}A zeolite for 1 h at 573–873 K. No uptake of hydrogen was observed; it was concluded that Co^{o} was not formed [24]. It was reported by Akbar [25] that attempts have been made to carry out the methanation reaction on CoA, CoX and CoY zeolites by adopting two procedures: one in which CO was introduced before H_2, and another in which CO was introduced after H_2. It was found that Co^{2+} zeolites were inactive in both procedures. In contrast with these results, the evidence here suggests that some reduction of Co^{2+} did occur in zeolite-A. Therefore, the formation of Co^{1+} is postulated.

The mechanism for the reduction of Co^{2+} to Co^{1+} is suggested to be that proposed by Herman *et al.* [1] for Cu^{2+} in zeolite-Y, i.e.

$$Co^{2+} + 1/2H_2 \rightarrow Co^{1+} + H^+ \quad (4)$$

The proton produced in the reduction (4) may react with skeletal oxygen to form an OH group:

$$H^+ + Z–O_1 \rightarrow Z–OH \quad (5)$$

According to Herman *et al.* [1], some of the lattice OH groups are assumed to be dehydroxylated at the experimental temperature of reduction:

$$2Z–OH \rightarrow H_2O + Z^+ + Z–O_1 \quad (6)$$

where *Z* represents an oxygen-deficient site in the framework of the zeolite.

Delafosse [26] showed that, when Ni^{2+} is reduced by hydrogen in X and Y zeolites, the metallic particles formed migrate towards the external surface and these particles rapidly increase in size with increase of the reduction temperature. Penchev *et al.* [27] investigated the reduction of Ni^{2+} in zeolite-A by means of XRD. They found that Ni aggregates on the external zeolite surface form metal crystals of considerable size. Therefore, the Co^{2+} after reduction is suggested here to migrate to the external surface or be localized in the intracrystalline surface of the zeolite. As a result of this migration, the 6-rings vacated by the migration of the reduced cobalt are filled by the Na^+ from the 8-rings.

The reduction peaks of the TPR profiles of CoA and NiA are centred at high-temperatures, showing that the metal cations are located in 6-rings and are more difficult to reduce. In the case of CuA, two reduction peaks are observed, centred at lower temperatures. According to Herman [1], the reduction of Cu^{2+} in CuNaY zeolites occurs via a two-step mechanism, as described before. After reduction at 200°C, only traces of water are formed and an amount of protons equivalent to the hydrogen consumed is formed. Since the reduction process involves the formation of OH groups, it is suggested that the stability arises from the inhibiting influence of acid groups adjacent to the Cu^+ species. Thus, further reduction of the Cu^+ produced from the initial Cu^{2+} is hindered by the close proximity of the product OH groups.

The ease of reduction is dependent on the location of the cations:

supercage > sodalite cage > hexagonal prism

The cations located in the supercages are reduced at low-temperature, and those in the sodalite cages are reduced at high temperatures. TPR data are given in Tables 3 and 4.

Table 3 TPR data on reduction of metal-exchanged zeolite-A

Sample	T_{max}/°C	Time/s	Intensity
CoA	686.7	6183	0.03906
NiA	625.3	5565	0.03125
CuA(I)	167.0	2229	0.03760
CuA(II)	290.7	3159	0.04053

Table 4 TPR data on reduction of metal-exchanged zeolite-A

Sample	Temperature range/°C	Hydrogen consumed/ μmol g^{-1}	Activation energy/ kJ mol^{-1}
CoA	575–700	26.87	344.80
NiA	300–700	60.48	170.00
CuA(I)	110–200	–	47.41
CuA(II)	200–550	64.06	131.40

The apparent activation energies of the reduction process were determined via the equation [23, 28]

$$2\ln T_m - \ln\beta + \ln[H_2] = \frac{E}{RT_m} + \text{constant} \quad (7)$$

where β is the heating rate, T_m is the reduction temperature and E is the activation energy of the reduction process. Values of T_m were obtained from the TPR spectrum by single graphical deconvolution. In order to reduce the errors due to the flow rate of hydrogen and the mass of solid, all TPR spectra were obtained under similar conditions. Figures 2–5 present plots of $(2\ln T_m - \ln\beta + \ln[H_2]_m)$ *vs.* $1/T_m$; the activation ener-

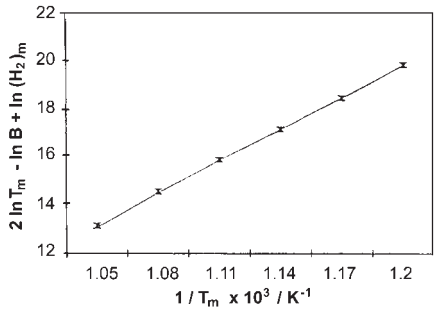

Fig. 2 Plot of $(2\ln T_m - \ln\beta + \ln[H_2]$ *vs.* $1/T_m$ for reduction of CoA

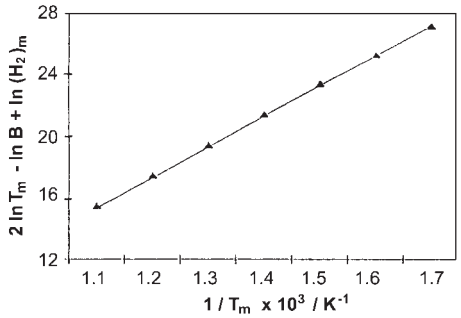

Fig. 3 Plot of $(2\ln T_m - \ln\beta + \ln[H_2]_m)$ *vs.* $1/T_m$ for reduction of NiA

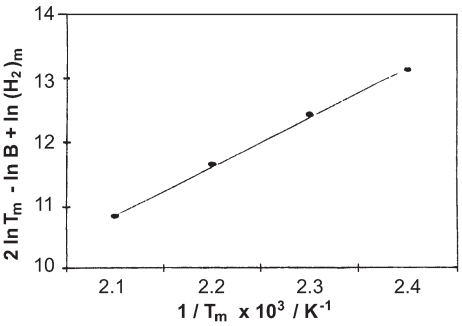

Fig. 4 Plot of $(2\ln T_m - \ln\beta + \ln[H_2]_m)$ *vs.* $1/T_m$ for reduction of CuA(I)

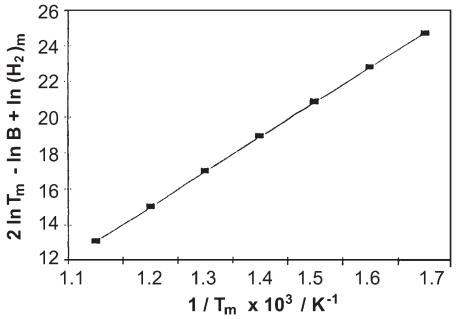

Fig. 5 Plot of $(2\ln T_m - \ln\beta + \ln[H_2]_m)$ *vs.* $1/T_m$ for reduction of CuA(II)

gies were calculated from the slopes of these lines (Table 2). The activation energy for CoA was 344.80 kJ mol^{-1}, that for NiA 170.00 kJ mol^{-1}, that for CuA at low-temperature 47.41 kJ mol^{-1} and that at high-temperature 131.40 kJ mol^{-1}. The TPR peak positions are at 167.0 and 290.7°C for CuA and at 686.7°C for CoA. The peak positions for CuA are more pronounced and sharp, while for CoA they are small and less conspicuous. From the plot of the standard free energy change as a function of temperature for the reduction process given by Hurst [23], it can be stated that the reduction process is more favourable for CuA than for NiA and CoA. ΔG^{o} is more

negative for CuA than for NiA and CoA. The standard electrode potential value for (Cu^{2+}, Cu) is +0.337 V, while those for (Ni^{2+}, Ni) and (Co^{2+}, Co) are –0.250 and –0.277 V, respectively. It is evident from these values that it is easier to reduce CuA than NiA or CoA. Thus, the difference in activation energy observed here reflects the difference in energy required to form a (H_2 – Cu^{2+}) transition state in the two lattice positions. It may be concluded that most of the metal cations, especially in the cases of Co^{2+} and Ni^{2+}, are located in the β-cavity of the zeolite.

References

1 R. G. Herman, J. H. Lunford, H. Beyer, P. A. Jacobs and J. B. Utterhoeven, J. Phys. Chem., 79 (1975) 2388.
2 H. Koller, A. R. Overweg, R. A. van Santen and J. W. de Haan, J. Phys. Chem. B, 101 (1997) 1754.
3 J. M. Thomas and C. William, J. Chem. Soc. Faraday Trans. I, 84 (1988) 2915.
4 A. W. Agofonov, Chem. Tech., 26 (1974) 9.
5 J. Blint, J. Phys. Chem. B, 100 (1996) 1958.
6 D. A. Fawx, W. Smith and T. R. Forester, J. Phys. Chem. B, 101 (1997) 1762.
7 G. C. Bond and S. P. Sarsam, Appl. Catal., 38 (1988) 365.
8 M. Afzal and F. Mahmood, Thermochim. Acta, 242 (1994) 265.
9 M. Afzal, F. Mahmood and S. Karim, J. Thermal Anal., 41 (1994) 1119.
10 J. C. White, J. B. Nicholas and C. H. Anthony, J. Phys. Chem. B, 101 (1997) 590.
11 P. Gallezat, Y. Ben Taarit and B. Imelik, J. Catal., 26 (1972) 295.
12 Kh. M. Minachev and Ya. I. Isakov, Zeolite Chemistry and Catalysis, Ed. J. A. Rabo (ACS monograph), 1976, p. 171.
13 J. B. Utterhoeven, Acta Phys. Chem., 24 (1978) 53.
14 H. Beyer, P. A. Jacobs and J. B. Utterhoeven, J. Chem. Soc., Faraday I, 72 (1976) 674.
15 M. Briend-Faure, J. Jeanjean, M. Kermarec and D. Delafosse, J. Chem. Soc. Faraday Trans. I., 74 (1978) 1538.
16 E. D. Garbowski and J. C. Vedrine, Chem. Phys. Lett., 48 (1977) 550.
17 E. D. Garbowski and M. Primet, Chem. Phys. Lett., 49 (1977) 247.
18 D. Barthomeuf, Molecular Sieves-II, Ed. J. R. Katzer, ACS Symp. Series 40, (1977) p. 457.
19 D. W. Breck, C. R. Caster and R. M. Milton, U. S. Pat. 3, 013, (1961) 990.
20 K. B. Herman and P. A. Jacobs, Molecular Sieves-II, Ed. J. R. Katzer, ACS Symp. Series 40 (1977) 493.
21 H. Beyer, P. A. Jacobs and J. B. Utterhoeven, J. Chem. Soc. Faraday Trans. I, 73 (1977) 1755.
22 B. Coughlan and K. A. Mark, J. Chem. Soc. Faraday Trans., 86 (1990) 1007.
23 S. J. Gentry, N. W. Hurst and A. Jones, J. Chem. Soc. Faraday Trans. I, 75 (1979) 1688.
24 D. Kallo, I. Preszler and K. Payer, J. Sci. Instr., 41 (1964) 338.
25 S. Akbar, Ph. D. Thesis, University of Bradford, U. K., 1980, p. 127.
26 J. Jeanjean, D. Delafosse and P. Gallezot, J. Phys. Chem., 83 (1979) 2761.
27 V. Penchev, N. Davidova, V. Kanzirev, H. Minchev and Y. Neinska, Adv. Chem. Ser., No. 121 (1973) 461.
28 P. Malet and A. Caballero, J. Chem. Soc. Faraday Trans. I, No. 7, 84 (1988) 2374.